

Article

Electronic Structure and Magnetism of Mn-Doped ZnO Nanowires

Fuchun Zhang ¹, Dandan Chao ¹, Hongwei Cui ¹, Weihu Zhang ¹ and Weibin Zhang ^{2,*}

¹ College of Physics and Electronic Information, Yanan University, Yanan 716000, China; E-Mails: yadxzfc@yau.edu.cn (F.Z.); yadxddc@163.com (D.C.); hweicui001@163.com (H.C.); ydzwh@163.com (W.Z.); wbzhang@dongguk.edu (W.Z.)

² Department of Physics, Dongguk University, Seoul 100-715, Korea

* Author to whom correspondence should be addressed; E-Mail: zmrright@163.com; Tel./Fax: +86-911-233-2045.

Academic Editor: Lorenzo Rosa

Received: 10 April 2015 / Accepted: 21 May 2015 / Published: 27 May 2015

Abstract: The geometric structures, electronic and magnetic properties of Mn-doped ZnO nanowires were investigated using density functional theory. The results indicated that all the calculated energy differences were negative, and the energy of the ground state was 0.229 eV lower than ferromagnetic coupling, which show higher stability in antiferromagnetic coupling. The calculated results indicated that obvious spin splitting phenomenon occurred near the Femi level. The Zn atoms on the inner layer of ZnO nanowires are easily substituted by Mn atoms along the [0001] direction. It was also shown that the $Mn^{2+}-O^{2-}-Mn^{2+}$ magnetic coupling formed by intermediate O atom was proved to be caused by orbital hybridization between Mn 3d and O 2p states. The magnetic moments were mainly attributed to the unpaired Mn 3d orbitals, but not relevant with doping position of Mn atoms. Moreover, the optical properties of Mn-doped ZnO nanowires exhibited a novel blue-shifted optical absorption and enhanced ultraviolet-light emission. The above results show that the Mn-doped ZnO nanowires are a new type of magneto-optical materials with great promise.

Keywords: ZnO; dilute magnetic semiconductors; nanowire; density functional theory; magnetic property

1. Introduction

Dilute magnetic semiconductors (DMSs) have attracted much attention due to their unique potential usage of both charge and spin of freedom of carriers in magneto-optical, magneto-electrical, and magneto-transport devices [1–4]. Especially, oxide-diluted magnetic semiconductors (such as ZnO) have shown excellent piezoelectric and photoelectric properties, and great potential applications in spintronic devices [5–7]. Moreover, theoretical and experimental research has predicted Curie temperatures (T_C) above room temperature, high solubility of magnetic ions, and transparency for visible light in ZnO-based DMSs [8,9]. In recent years, great progress has been achieved in one-dimensional (1D) ZnO-based DMSs. Chang *et al.* [10] prepared $Zn_{1-x}Mn_xO$ nanowires (NWs) at 500 °C with a high doped content of 13%. Philipose *et al.* [11] also successfully prepared $Zn_{1-x}Mn_xO$ NWs, and the samples showed stable ferromagnetic (FM) and ultraviolet emission properties. Wang *et al.* [12] prepared $Zn_{1-x}Mn_xO$ NWs and no second phase was observed in the Mn-doped ZnO NWs. Theoreticians have found ZnO to be an excellent candidate host semiconductor for high- T_C ferromagnetism. Dietl *et al.* [2] made theoretical predictions about the higher Curie temperature of Mn-doped ZnO, Sato *et al.* [13] revealed the magnetic properties of 3d TMs-doped ZnO by using the local density approximation (LDA). Marcel *et al.* [14] investigated the ferromagnetic (FM) and antiferromagnetic (AFM) properties of 3d TMs-doped ZnO. Our previous studies have shown that potential FM ground states are more stable in V-doped and Fe-doped ZnO NWs [15,16], and have obvious half-metallic properties in Fe-doped ZnO NWs [16]. In addition, He *et al.* [17] have reported on the electronic and magnetic properties of Mn-doped ZnO nanotubes using density functional theory (DFT) with the generalized gradient approximation (GGA). However, many problems in the research of ZnO-based DMSs still remain both scarce and controversial regarding the influence of impurities on the electronic, optical, and magnetic properties. The magnetic coupling mechanism and origin of the ferromagnetism is still not clear, and experimental observations demonstrate controversial results about optical phenomenon in the optical absorption with regards to Mn-doped ZnO NWs. In order to clarify the effect of Mn doping on the electronic, optical, and magnetic properties of ZnO NW, it is necessary to perform first-principles methods based on DFT.

In this paper, the geometric structures, and electronic and magnetic properties of Mn-doped ZnO NWs were systematically investigated by first-principles methods, based on DFT. The applicable methods to adjust and control oxide DMSs were obtained by analysis of the magnetic coupling mechanism of Mn-doped ZnO NWs. We systematically study mechanisms of FM and AFM coupling on the electronic, optical, and magnetic properties. The main results provide theoretical guidance for preparing ZnO-based DMS materials of high quality and high- T_C .

2. Theoretical Models and Calculated Methods

The models for Mn-doped ZnO NWs are generated from a wurtzite ZnO ($7 \times 7 \times 2$) supercell structure along the [0001] direction (see Figure 1a). All atoms within the dashed line remained to build up the ZnO NW structure in Figure 1b. Our NW model contains 96 atoms ($Zn_{46}Mn_{2}O_{48}$). The vacuum region of ZnO NWs along [0110] and [1010] is 15 Å to avoid the effects of the interaction between Mn-doped ZnO NWs on the results, and we select the periodical structure along [0001] direction, as

shown in Figure 1b. To investigate the magnetic coupling mechanism between the two Mn atoms, we replace two of the Zn atoms with Mn in ZnO NWs. The six possible magnetic coupling models are shown in Figure 2, and Mn doping concentration is at 4.2%.

The calculations were carried out by using the first principles methods based on DFT, additionally, the Vienna *Ab initio* Simulation Package (VASP) was applied in our work [18]. The detailed parameters were set as follows, the exchange-correlation function was calculated based on GGA in the form of the Perdew-Burke-Ernzher (PBE) [19], the valence electronic configuration of O, Zn and Mn atoms were $2s^22p^4$, $4s^23d^{10}$ and $4s^23d^5$, respectively, the cut-off energy of plane wave was set at 420 eV, and the convergence in energy and force was less than 1×10^{-5} eV and 10^{-3} eV/Å, respectively, and the stress on the cell was less than 0.01 GPa. The Brillouin zone was sampled with a mesh of $1 \times 1 \times 16$ k points, generated by the Monkhorst-Pack scheme.

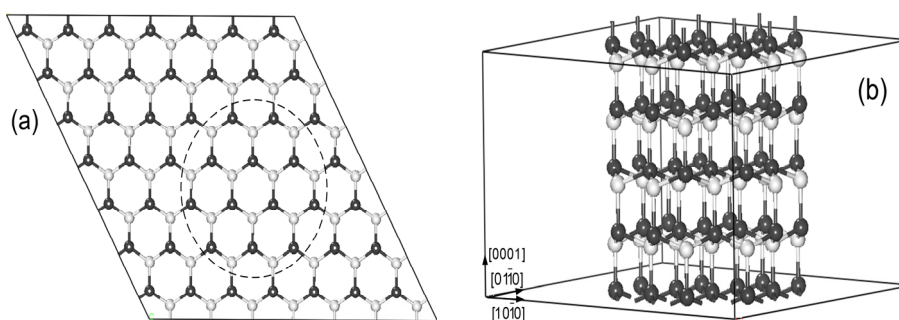


Figure 1. (a) The top view of the $7 \times 7 \times 2$ ZnO supercell structure; (b) $Zn_{48}O_{48}$ nanowires (NWs) supercell along the [0001] direction (The white and black spheres represent O and Zn atoms).

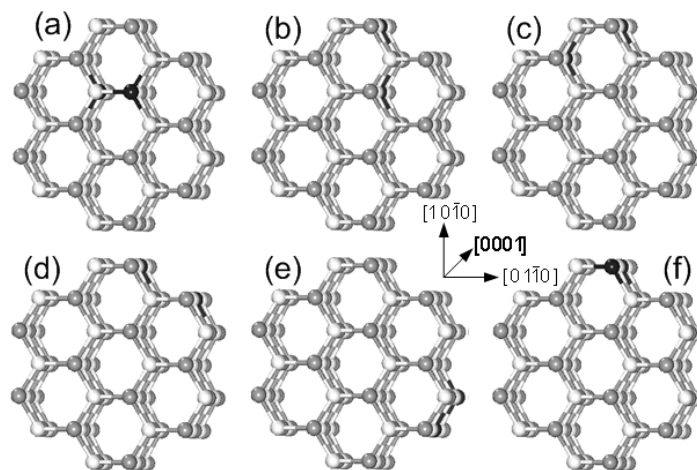


Figure 2. The structures of Mn-doped ZnO NWs. (a) Configuration I; (b) Configuration II; (c) Configuration III; (d) Configuration IV; (e) Configuration V; (f) Configuration VI. (The white, gray, and black spheres represent O, Zn, and Mn atoms, respectively).

3. Results and Discussion

To verify the geometric structure, and electronic and magnetic properties of the Mn-doped ZnO NWs, the geometric structures and electronic properties of pure $Zn_{48}O_{48}$ NW were calculated under

full geometry relaxation. The total energy of the optimized ZnO NW was found to be 6.371 eV lower than that of the unoptimized one. The optimized Zn–O bond length along the [0001] direction was 1.899 Å on the outermost surface layer, which was 4.67% shorter than that of bulk ZnO. The optimized Zn–O bond lengths were 1.969 Å and 1.978 Å on the inner-layer NWs, and 1.15% and 0.7% shorter than that of bulk ZnO, respectively. The optimized Zn–O bond lengths along the $[0\bar{1}10]$ direction were between 1.955 Å and 1.962 Å on the outermost surface layer, their corresponding bond angles of $\angle\text{O–Zn–O}$ (108.04°) and $\angle\text{Zn–O–Zn}$ (108.04°) changed into $\angle\text{O–Zn–O}$ (113.76°) and $\angle\text{Zn–O–Zn}$ (105.81°). In addition, it was observed from Figure 3a that the total density of states (DOS) for the spin-up and spin-down were identical, namely, pure ZnO NW is a nonmagnetic material. The calculated band gap was 1.86 eV, which was significantly larger than that of our calculated bulk ZnO (0.97 eV).

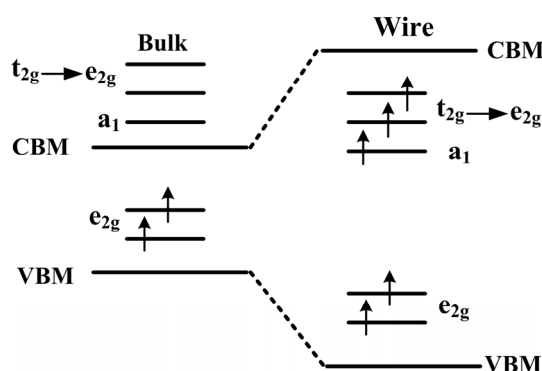


Figure 3. The schematic plot of 3d level splitting in the ZnO bulk and NW.

Table 1 illustrates the magnetic coupling modes, geometric parameters, energy, bond lengths, and magnetic moments of Mn-doped ZnO NW, in which ΔE ($\Delta E = E_{AFM} - E_{FM}$) denotes energy difference after optimized treatments, ΔE_0 ($\Delta E = E_{AFM} - E_{FM}$) denotes the unoptimized energy difference, and the relative energy $\Delta\varepsilon$ denotes the energy difference corresponding to the ground state configuration. As shown in Table 1, the ΔE of Mn-doped ZnO NWs are all negative, which indicates that the AFM states are more stable than FM states. The configuration V corresponds to the ground state of Mn-doped ZnO nanowires, and its energy is lower than FM state energy by 0.229 eV. In this configuration, the two Mn atoms reside in the inner layer sites along the [0001] direction. As for configuration VI, the energy difference ΔE is only -0.007 eV, which indicates that AFM coupling is slightly more stable than FM coupling. In order to further investigate AFM interactions, we note that the corresponding energies of FM and AFM states are almost same as shown in Table 1 ($\Delta E = -0.007$ eV), and the AFM coupling is weak with the increase of Mn–Mn bond length for configuration VI ($d_{\text{Mn–Mn}} = 5.205$ Å). Hence, it is prone to forming a paramagnetic state and spin-glass state. It is indicated that the Mn–O bond length may play a more important role than the Mn–Mn bond length in predicting the magnetic coupling, which suggests that the range of magnetic interactions between the two Mn atoms is rather short and independent of the Mn–Mn distance. While configurations II, III, and IV are in an AFM state for Mn-doped ZnO nanowires along other directions. Our calculated results are consistent with previously reported results [11,20–22]. Moreover, all magnetic moments of Mn atoms are 3.947–4.193 μ_B and mainly originate from 3d electrons of Mn

atoms. Oxygen atoms also show AFM spin polarization in nearest-neighbor Mn atoms, which produce a weak magnetic moments of -0.061 – $-0.089 \mu_B$. As for the relaxed geometric structure, the calculated results show that the Mn–O and Mn–Mn bond lengths are 1%–3% shorter than that of an unrelaxed one. The outer layer of ZnO NWs shows more intense relaxation than the inner one, therefore presenting high surface effects and quantum size effects.

Table 1. Magnetic coupling modes, energy, bond lengths, and magnetic moments.

Modes	ΔE (eV)	ΔE_0 (eV)	$\Delta \varepsilon$ (eV)	Coupling	$d_{\text{Mn-O}}$ (Å)	$d_{\text{Mn-Mn}}$ (Å)	Mn ₁ (μ_B)	Mn ₂ (μ_B)	O (μ_B)
I	-0.302	-0.052	0.721	AFM	1.914	3.134	4.171	-4.176	-0.061
II	-0.219	-0.053	0.208	AFM	1.819	3.111	4.134	-4.070	-0.069
I	-0.144	-0.047	0.405	AFM	1.916	3.060	3.947	-4.113	-0.074
IV	-0.139	-0.095	0.561	AFM	1.816	3.264	4.021	-4.104	-0.071
V	-0.229	-0.061	0.000	AFM	1.839	2.694	4.078	-4.067	-0.070
VI	-0.007	-0.003	0.117	AFM	1.823	5.205	4.193	-4.021	-0.089

To further study the origin of magnetic coupling between two Mn atoms, Figure 3 displays the schematic of splitting 3d level occupation in bulk ZnO and NW. For Mn-doped ZnO NW, the positions of Zn²⁺ ions are replaced by Mn²⁺ ions, and an Mn²⁺ (*d*⁵ configuration) ion has a tetrahedral structure in a crystalline field. The 3d states of an Mn atom split into one upper, triply degenerate *t*_{2g} state (*d*_{xy}, *d*_{yz}, *d*_{xz}) and one lower, doubly degenerate *e*_g state (*d*_{z²-r²}, *d*_{x²-y²}). However, the space group of ZnO with a wurtzite structure degrades from a high symmetric *T*_d to a *C*_{3v} group in the NW, the *t*_{2g} states are no longer the original triply degenerate, but further divide into one doubly degenerate *e*_{2g} state and one singly *a*₁ state. In particular, O 2*p* states also splits into an *e*_g state and an *a*₁ state, due to the high symmetry of *T*₂ in O 2*p* orbital. Magnetic coupling between O 2*p* and Mn 3d states cause localization characteristics of the *e*_g states owing to the same symmetry. Figure 4 shows the FM and AFM mechanisms of the Mn-doped ZnO NW. According to the Hund rules and the Pauli exclusion principle, the two lower *e*_g levels located in the gap are fully occupied in the upper-spin bands, and pushed upward and downward by the same Δd to form an FM coupling when there is no energy input, as shown in Figures 3 and 4a. For the AFM coupling in Figure 4a, the upper-spin *e*_g level of Mn ion couples with that of another Mn ion with the same level, the occupied *e*_g levels are pushed up by Δd energy, and the unoccupied ones are pushed down by Δd energy due to the half-occupation of the *e*_g levels, as shown in Figure 4b, thus, the super-exchange interaction is smaller than the double exchange interaction. By increasing distance between the two Mn²⁺ ions, the AFM coupling of d-d state becomes weaker, and the doped system can form paramagnetic or spin-glass states, which is consistent with our analysis about geometric structure and stability in previous section. The Mn-doped ZnO nanowires show an AFM behavior, and are prone to form a zigzag chain of Mn–O–Mn atoms along the [0001] direction, which indicate that the doped systems have a good effect on the [0001] preferred orientation to prepare ZnO-based dilute magnetic semiconductors.

In order to further explain the magnetic coupling of Mn-doped ZnO NW, Figure 5 shows the total density of states (TDOS) and partial density of states (PDOS) of FM and AFM states. It can be seen that the TDOS of Mn-doped ZnO NW moves towards low energy (0.95 eV), and one can see that the

spin-up Mn 3d states pass through the Fermi level for FM states, which confirms that the doped system is a half-metallic ferromagnet and exhibits 100% spin polarization. The strong FM coupling between the Mn 3d and O 2p states occurs at the top valence band (−1.0–0 eV) and the bottom valence bands (−4.0–−7.0 eV), the dispersive bonding t_{2g}^b state and the local nonbonding e_g^e state is formed at the valence band (−2–−6 eV) and near the Fermi level, respectively. The antibonding t_{2g}^a state is formed at the conduction band (1.6–2.1 eV). In particular, one can see from Figure 5c that the role of the O atom mediates the magnetic coupling between Mn atoms. The magnetic coupling chains of $\text{Mn}^{2+}\text{--O}^{2-}\text{--Mn}^{2+}$ would reveal a double exchange mechanism owing to impurity states in the gap region. On the other hand, the magnetic moments of Mn atoms are 4.012–4.193 μ_B and mainly come from the Mn 3d orbitals, which are less than the theoretical value of 5 μ_B . However, small contributions to the magnetic moments come from O 2p orbitals. As for AFM state, we find that the spin-up and spin-down DOS are asymmetrical, the spin-up electrons are more than the spin-down electrons. As the DOS of spin-up and spin-down states all pass through the Fermi level, the AFM state is a possible metal ferromagnet. Spin-exchange splitting is also observed between Mn 3d and O 2p states, as shown in Figure 5e,f. Thus, the local bonding t_{2g}^b states are fully occupied between −1.5 eV and −1.0 eV. Whereas the nonbonding t_{2g}^a states are 4/5 occupied between −1.0 eV and the Fermi level, the anti-bonding e_g^e states are full empty between 0.6 eV and 2.5 eV, which correspond to the Mn 3d states. We note that the bandwidth of the bonding and antibonding band is greatly narrowed for AFM states, and the spin-orbital coupling and hybridization effects are significantly higher than FM states. Therefore, stable AFM states can be easily formed in Mn-doped ZnO NWs. This is mainly because the Mn^{2+} ($3d^5$) ion shows a half-full 3d electronic configuration, the spin-up 3d orbitals of Mn^{2+} atom are all occupied, and there are no excessive unoccupied orbitals for hybridization coupling with neighboring Mn^{2+} ions. As a result, 3d orbital electrons of the neighboring Mn^{2+} are prone to filling the levels along the reverse parallel direction, which is in accordance with the mechanisms shown in Figures 3 and 4. In addition, the up-spin or down-spin orbitals are fully empty for the higher e_{2g} state and AFM coupling is favored. Namely, the AFM coupling can be formed more easily in Mn-doped ZnO NWs according to theoretical analysis, which is similar to the reported results [23,24].

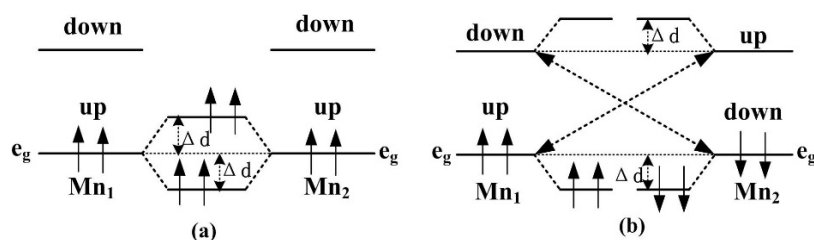


Figure 4. The ferromagnetic (FM) and antiferromagnetic (AFM) mechanisms of the Mn-doped ZnO NW. (a) FM coupling; (b) AFM coupling.

The optical absorption spectrum of Mn-doped ZnO NWs is illustrated in Figure 6. We applied the scissors operator ($E_{scissor} = 1.51$ eV) to adjust the experimental and calculated band gap based on the experimental result (3.37 eV). To study the effect of Mn-doped on the optical properties, the absorption spectrum of pure ZnO NWs is also calculated. Some previous experimental studies [25–27] found that pure ZnO NW shows a strong absorption peak in the ultraviolet region as a result of

near-band edge absorption. A wide green-yellow luminous bands form within the visible region of 550–600 nm. As shown in Figure 6, the calculated optical properties show that the absorption spectrum of the Mn-doped ZnO NWs are blue-shifted in the ultraviolet region, and the broad ultraviolet emission from 320 nm to 340 nm is observed in a doped system, which is related to electron transitions from the top valence band to the bottom conduction band. The calculated result is similar to the reported experimental optical absorption spectra of Mn-doped ZnO nanoparticles [28,29] and Mn-doped ZnO nanowires [30,31]. Additionally, one “sharp” absorption peak appears in the far-ultraviolet region near 90 nm, which are transitions from the s - d and p - d coupling of localized Mn $3d$ orbitals. The increase in the intensity of the UV peak is considered to be due to the participation of the $3d$ electrons of Mn [10,29,30], and is very similar to Co-doped ZnO nanowires [32]. The above-calculated results indicate a strong photo-response for ultraviolet-light luminescence. Namely, the Mn-doped ZnO NWs may be a new type of magneto-optical material with great promise.

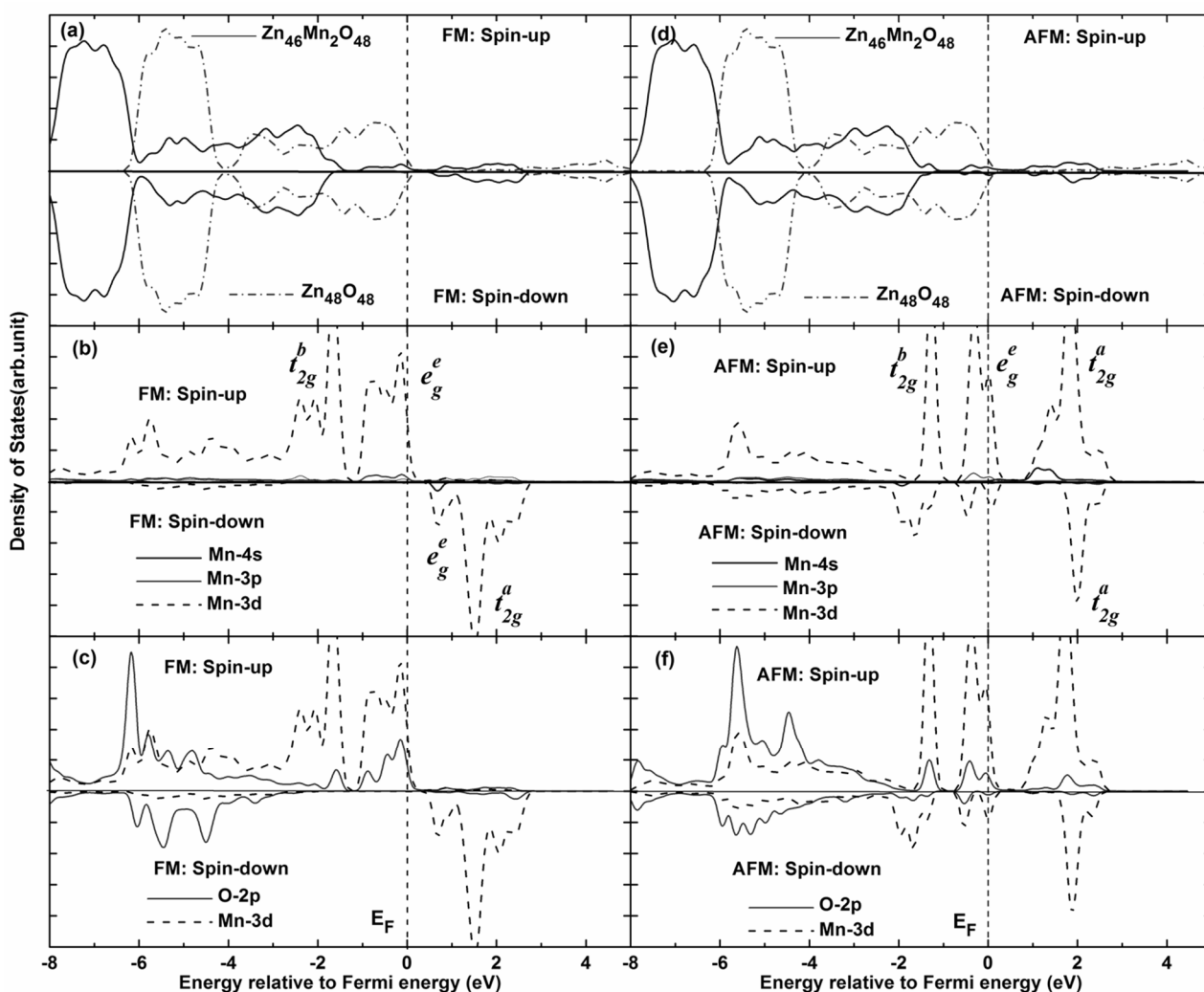


Figure 5. Total density of states (TDOS) and partial density of states (PDOS) of Mn-doped ZnO NW. (a) TDOS of pure $Zn_{46}O_{48}$ and Mn-doped ZnO nanowire for FM states; (b) PDOS of Mn atom for FM states; (c) PDOS of Mn $3d$ and O $2p$ for FM states; (d) TDOS of pure $Zn_{46}O_{48}$ and Mn-doped ZnO nanowire for FM states; (e) PDOS of Mn atom for AFM states; (f) PDOS of Mn $3d$ and O $2p$ for AFM states.

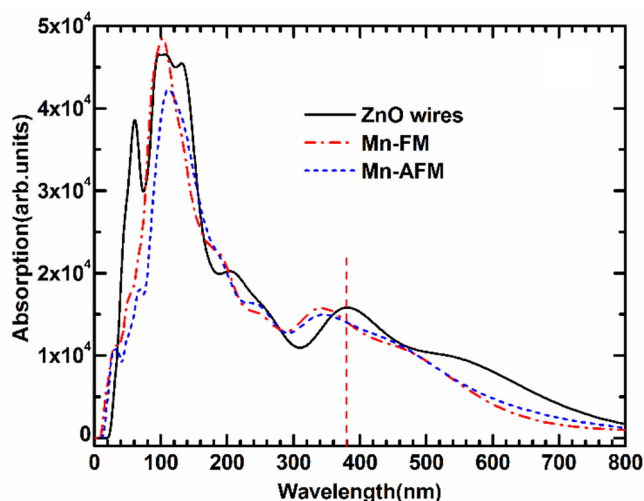


Figure 6. The optical absorption curves of FM and AFM for Mn-doped ZnO NW.

4. Conclusions

In summary, geometric structures, and electronic and magnetic properties of Mn-doped ZnO NWs were investigated by using first-principles methods based on DFT. The magnetic origination and magnetic coupling mechanism were analyzed in detail. The results indicate that AFM coupling is the most stable for six doping configurations, and $p-d$ hybridization coupling occurred at the top valence bands between Mn $3d$ and O $2p$ states. The dispersive bonding state and local nonbonding state are formed in valence bands, and a local antibonding state is formed in conduction bands. Magnetic moments are originated mainly from Mn $3d$ orbitals. The theoretical results further reveal the half-metallic magnetic properties of FM coupling and metallic magnetic properties of AFM coupling. Our research will provide theoretical guidance for preparing ZnO-based DMSs with a high Curie temperature.

Acknowledgments

The authors thank all colleagues who contributed to the results described in this article and whose names appear in joint publications. This research was supported by the National Natural Science Foundation of Shaanxi Province, China (2014JM2-5058), the Scientific Research Program of Yan'an city, China (2013-KG03), the Science Innovation Training Program (2014107191081) and the Science Foundation of Yan'an University (YD2014-02).

Author Contributions

The FZ and WZ conceived and designed the study. The DC and HC performed the theoretical calculation and edited the manuscript. The FZ wrote the manuscript.

Conflicts of Interest

The authors declare no conflict of interest.

References

1. Ohno, H. Making nonmagnetic semiconductors ferromagnetic. *Science* **1998**, *281*, 951–954.
2. Dietl, T.; Ohno, H.; Matsukura, F.; Cibert, J.; Ferrand, D. Zener model description of ferromagnetism in zinc-blende magnetic semiconductors. *Science* **2000**, *287*, 1019–1022.
3. Pan, Z.W.; Dai, Z.R.; Wang, Z.L. Nanobelts of semiconducting oxides. *Science* **2001**, *281*, 1947–1949.
4. Huang, M.H.; Mao, S.; Feick, H.; Yan, H.Q.; Wu, Y.Y.; Kind, H.; Weber, E.; Russo, R.; Yang, P.D. Room-temperature ultraviolet nanowire nanolasers. *Science* **2001**, *292*, 1897–1899.
5. Ye, C.Q.; Li, M.Z.; Luo, J.; Chen, L.F.; Tang, Z.M.; Pei, J.; Jiang, L.; Song, Y.L.; Zhu, D.B. Photo-induced amplification of readout contrast in nanoscale data storage. *J. Mater. Chem.* **2012**, *22*, 4299–4305.
6. Chau, R.; Doyle, B.; Datta, S.; Kavalieros, J.; Zhang, K. Integrated nanoelectronics for the future. *Nat. Mater.* **2007**, *6*, 810–812.
7. Ma, X.; Tian, H. Bright functional rotaxanes. *Chem. Soc. Rev.* **2010**, *39*, 70–80.
8. Jin, Z.W.; Fukumura, T.; Kawasaki, M.; Ando, K.; Saito, H.; Sekiguchi, T.; Yoo, Y.Z.; Murakami, M.; Matsumoto, Y.; Hasegawa, T.; *et al.* High throughput fabrication of transition-metal-doped epitaxial ZnO thin films: A series of oxide-diluted magnetic semiconductors and their properties. *Appl. Phys. Lett.* **2001**, *78*, 3824.
9. Norberg, N.S.; Kittilstved, K.R.; Amonette, J.E. Synthesis of colloidal Mn²⁺:ZnO quantum dots and high-TC FM nanocrystalline thin films. *J. Am. Chem. Soc.* **2004**, *126*, 9387–9398.
10. Chang, Y.Q.; Wang, D.B.; Luo, X.H.; Xu, X.Y.; Chen, X.H.; Li, L.; Chen, C.P.; Wang, R.M.; Xu, J.; Yu, D.P. Synthesis, optical, and magnetic properties of diluted magnetic semiconductor Zn_{1-x}Mn_xO nanowires via vapor phase growth. *Appl. Phys. Lett.* **2003**, *83*, 4020–4022.
11. Philipose, U.; Naira, S.V. High-temperature ferromagnetism in Mn-doped ZnO nanowires. *Appl. Phys. Lett.* **2006**, *88*, 263101.
12. Zhang, X.M.; Zhang, Y.; Wang, Z.L. Synthesis and characterization of Zn_{1-x}Mn_xO nanowires. *Appl. Phys. Lett.* **2008**, *92*, 162102.
13. Sato, K.; Katayama, H. Material design for transparent ferromagnets with ZnO-Based Magnetic Semiconductors. *Jpn. J. Appl. Phys.* **2000**, *39*, L555–L558.
14. Sluiter, M.H.F.; Kawazoe, Y.; Sharma, P.; Inoue, A.; Raju, A.R.; Rout, C.; Waghmare, U.V. First principles based design and experimental evidence for a ZnO-based ferromagnet at room temperature. *Appl. Phys. Lett.* **2005**, *94*, 187204.
15. Zhang, F.C.; Dong, J.T.; Zhang, W.H.; Zhang, Z.Y. Ferromagnetism of V-doped ZnO nanowires. *Chin. Phys. B* **2013**, *22*, 027503.
16. Zhang, F.C.; Zhang, W.H.; Dong, J.T.; Zhang, Z.Y. First-principles study of Fe-doped ZnO nanowires. *Chin. Phys. Lett.* **2011**, *28*, 126102.
17. He, A.L.; Wang, X.Q.; Fan, Y.Q.; Feng, Y.P. Electronic structure and magnetic properties of Mn-doped ZnO nanotubes: An *ab initio* study. *J. Appl. Phys.* **2010**, *108*, 084308.
18. Kresse, G.; Furthmüller, J. Efficient iterative schemes for *ab initio* total-energy calculations using a plane-wave basis set. *Phys. Rev. B* **1996**, *54*, 011169.

19. Kresse, G.; Joubert, D. From ultrasoft pseudopotentials to the projector augmented-wave method. *Phys. Rev. B* **1999**, *59*, 1758–1775.
20. Baik, J.M.; Lee, J.L. Fabrication of vertically well-aligned (Zn, Mn)O nanorods with room temperature ferromagnetism. *Adv. Mater.* **2005**, *22*, 2745–2748.
21. Zhu, Y.H.; Xia, J.B. Electronic structure of Mn-doped ZnO quantum wires: A mean-field theory study. *Phys. Rev. B* **2007**, *75*, 205113.
22. Pradhan, A.K.; Zhang, K.; Mohanty, S.; Dadson, J.B.; Hunter, D. High-temperature ferromagnetism in pulsed-laser deposited epitaxial (Zn, Mn)O thin films: Effects of substrate temperature. *Appl. Phys. Lett.* **2005**, *86*, 152511.
23. Lawes, G.; Risbud, A.S.; Ramirez, A.P.; Seshadri, R. Absence of ferromagnetism in Co and Mn substituted polycrystalline ZnO. *Phys. Rev. B* **2005**, *71*, 045201.
24. Prashant, K.S.; Ranu, K.D.; Choudhary, R.J.; Pandeya, A.C. Doping, strain, defects and magneto-optical properties of $Zn_{1-x}Mn_xO$ nanocrystals. *CrystEngComm* **2013**, *15*, 4438–4447.
25. Zhang, Z.H.; Qi, X.Y.; Jian, J.K.; Duan, X.F. Investigation on optical properties of ZnO nanowires by electron energy-loss spectroscopy. *Micron* **2006**, *37*, 229–233.
26. Kong, Y.C.; Yu, D.P.; Zhang, B.; Fang, W.; Feng, S.Q. Ultraviolet-emitting ZnO nanowires synthesized by a physical vapor deposition approach. *Appl. Phys. Lett.* **2001**, *78*, 407–410.
27. Chen, T.; Xing, G.Z.; Zhang, Z.; Chen, H.Y.; Wu, T. Tailoring the photoluminescence of ZnO nanowires using Au nanoparticles. *Nanotechnology* **2008**, *19*, 435711.
28. Hao, Y.M.; Lou, S.Y.; Zhou, S.M.; Yuan, R.J.; Zhu, G.Y.; Li, N. Structural, optical, and magnetic studies of manganese-doped zinc oxide hierarchical microspheres by self-assembly of nanoparticles. *Nano. Res. Lett.* **2012**, *7*, doi: 10.1186/1556-276X-7-100.
29. Yang, L.W.; Wu, X.L.; Huang, G.S.; Qiu, T.; Yang, Y.M. *In situ* synthesis of Mn-doped ZnO multileg nanostructures and Mn-related Raman vibration. *J. Appl. Phys.* **2005**, *97*, 014308.
30. Phan, T.; Sun, Y.; Vincent, R.; Cherns, D.; Nghia, N.; Yu, S.-C. Optical properties of Mn-doped ZnO nanowires. *J. Korean Phys.* **2008**, *52*, 1633–1636.
31. Deka, S.; Joy, P.A. Synthesis and magnetic properties of Mn doped ZnO nanowires. *Solid State Commun.* **2007**, *142*, 190–194.
32. Chang, Y.Q.; Wang, P.W.; Ni, S.L.; Long, Y.; Li, X.D. Influence of Co content on raman and photoluminescence spectra of Co doped ZnO nanowires. *J. Mater. Sci. Technol.* **2012**, *28*, 313–316.